International Journal of Engineering Innovation & Research
Volume 3, Issue 4, ISSN: 2277 – 5668

An Efficient Switched Filter Compensation Low-Impact Scheme for EV-DC Drives

E. Elbakush
Electrical & Computer Engineering Sharaf Energy Systems, Inc.
University of New Brunswick Fredericton, NB, Canada
Email: e.elbakush@unb.ca

A. M. Sharaf
Electrical & Computer Engineering Sharaf Energy Systems, Inc.
University of New Brunswick Fredericton, NB, Canada
Email: profdramsharaf@yahoo.ca

Abstract **– This paper presents a new switched filter scheme and coordinated control strategy for a permanent magnet DC (PMDC) electric vehicle (EV) with an energy recovery free- wheeling scheme. The integrated DC drive scheme is fully stabilized using a FACTS-based efficient switched filter compensator (ESFC) that ensures a fully stabilized VD Bus voltage with reduced inrush current conditions under source and load excursions. The Lithium-ion battery is utilized efficiently using the error-driven multi-loop control strategy. The EV drive scheme is validated using a tri-loop weighted modified proportional integral derivative (WMPID) controller to control the DC/DC converter and the efficient recovery switched filter scheme. The paper presents the validation of the multi-loop WMPID controller for the Lithium-ion battery scheme for four-wheel DC drive using PMDC motors. The tri-loop dynamic error regulator is used to regulate the motor inrush current and prevent overload conditions, in addition to speed dynamic reference tracking. A four-quadratic DC/DC converter is employed to control the transient energy exchange from the Lithium-ion battery to the PMDC motor load. The second controller is a DC voltage dynamic tracking controller using the FACTS-based ESFC. The Lithium- ion battery, DC/DC converter, PMDC motor, and controller loops are fully modelled using the MATLAB/Simulink/Sim-powerSystemtoolbox environment.**

Keywords **– Dual Regulation Weighted Modified PID Controller, Efficient Switched Filter Compensator (ESFC), Electric Vehicles, Lithium-Ion Battery.**

I. INTRODUCTION

Highlight Lately, EVs have attracted a great deal of interest and are being marketed as a practicable solution to emerging energy concerns and environmental issues. These prospects have stimulated a great deal of research and development intended to make EVs practical. With improved motors and batteries, some EVs already perform extremely well, even when compared with internal combustion engine vehicles (ICVs) [1]. EVs are driven by AC and DC electric motors powered by rechargeable batteries. Electric motors have several advantages over internal combustion engines (ICEs). The EVs' power electronics and connected control systems are the system components that will make EVs' technology practicable [2], [3], [4].

The transportation sector is one of the major contributors to fossil fuel energy demand, air pollution, and greenhouse gases, which are major issues in view of the challenges associated with the supply of oil and expected higher gasoline prices, as well as tighter emission requirements. Therefore, the subject of alternative fuels for meeting the future energy demand of the transport sector has gained much attention due to the present energy and environmental concerns [5].

The main elements of EVs in general are the battery and drive system. The battery stores energy to be released when needed. The battery with DC-DC interface allows regenerative braking in the EVs and allows complementing a slow dynamic energy source, such as the fuel cell (FC). Benefits are drawn from these features in EVs based on FCs such as the Honda FCX Clarity. The battery management system (BMS) must ensure efficient management of the battery's state of charge (SOC). To accomplish this, the designer of the BMS must have a detailed simulation of the EV's traction system including a detailed model of the battery [6], [7], [8].

Recently, EV technology and market penetration have been sustained by a need to reduce fossil fuel energy demand and climate change due to carbon dioxide emissions, and decrease dependence on fossil fuels and combustion engine vehicles. Accordingly, the more effective and convenient solution is using the new generation of green electric vehicles (GEVs), which are charged by electric energy obtained from renewable energy sources. EVs are supplied by batteries, which can be recharged through connecting to external power sources. An exceptional issue in this regard is that these sources can be renewable energy supplies such as photovoltaic (PV) arrays, FC, and wind that feed EVs in vehicle-to-grid (V2G) power stations and vehicle-to-house (V2H) schemes [9], [10], [11], [7]. Several types of electric motors may be used for EV propulsion purposes. Earlier traction motors were exclusively DC motors, either series-excited or separately-excited. Recently, more advanced AC drive systems have foundapplication in EV propulsion using induction motors, permanent magnet synchronous motors, and permanent magnet brushless DC motors [12], [13].

Switched and active power filters (APF) and FACTS switched filter compensator devices have been proposed to increase power quality, eliminate line current harmonics, and improve power factor [14]. Accordingly, these devices can modify power factor and harmonic distortion in smart grids and battery charging systems. Taking this idea into account, a FACTS-based filter is proposed for plug-in hybrid and electric vehicles. A multi-loop dynamic error-driven time- descaled weighted modified proportional integral derivative (WMPID) controller regulates the ESFC resulting in efficient, low-impact scheme for EV-DC drives, in order to achieve the best performance. The

design challenge is the development of a fast dynamic control system that can stabilize the common DC Bus voltage and reduce inrush current conditions. The useof FACTS technology and power electronic devices can meet this challenge [15], [16], [17].

In this paper, the Lithium-ion battery scheme powering the PMDC EV motor drive system is fully studied. A PMDC motor is located on each wheel of the four-wheel EV and operated in full synchronism under various control strategies. The proposed EV scheme is controlled by a number of dynamic time decoupled control strategies. The WMPID regulating algorithms are utilized to track any reference speed trajectory under varying parameters and load conditions. The control system comprises four different regulators to track speed reference trajectory with minimum over/under current, inrush, and ripple conditions. The proposed optimized time descaled and decoupled control scheme has been tested for effective dynamical speed reference trajectory tracking, efficient power utilization, limited inrush current conditions, and reduced DC side transients and voltage excursions.

II. Sample Study System

Figures 1 - 2 show the proposed EV all-wheel PMDC-drive system scheme with the Lithium-ion battery. The proposed drive system consists of six parts. These are Lithium-ion battery, efficient switched filter compensator, DC/DC chop- per, four PMDC drive motors, a free-wheel diode, and DC load. The DC compensator scheme is used to ensure stable, efficient, minimal inrush operation of the hybrid renewable energy scheme. The WMPID multi-regulators and coordinated controller are used for the following purposes:

1) Efficient switched filter compensator regulator for pulse width switching scheme to regulate the DC Bus voltage and minimize inrush current transients and non-linear volt-ampere load excursions characteristics. The ESFC device acts as a matching DC/DC interface device between the DC load dynamic characteristics.
2) The speed regulator of the permanent magnet DC motor drive ensures speed reference tracking with minimum inrush conditions and ensuring reduced voltage transients and improved energy utilization.

III. Efficient Switched Filter Compensator (ESFC)

In order to improve an efficient low-impact scheme for EV- DC drive performance, an efficient switched filter compensator comprising switchable capacitor is introduced at the DC Bus. The ESFC is also controlled to absorb ripple and reduce DC side current oscillations. The idea behind the controller is to detect major excursions in the motor and feed the errors to a pulse width modulated (PWM) block that in turn generates the switching pulses for the filter switches in accordance with the duty ratio and the error value [18]. The ESFC used and tested with the operation of the electric motor is shown in Figure 2. The ESFC control scheme is based on decoupled current and voltage components of the DC Bus. The ESFC must be connected across the DC Bus terminal to maintain constant DC voltage in order to allow operation of the WMPID controller with three control loops as shown in the Simulink model in Figure 3. The primary duty of the capacitor bank is to provide a voltage path, current path, and power path as shown in Figure 5. The input of control loop 1 is the Bus voltage, which produces an error with respect to the measured value, and then the error is used for voltage regulation. The input to loop 2 is the Bus current that has the same transfer function as the voltage loop. The input to loop 3 is the power loop that has the same transfer function as the voltage loop. The increased capacity of power electronic converters used in ESFC also allows for adequate sizing and optimized operation [18]. In this paper the effectiveness of the ESFC scheme is fully validated using MATLAB /Simulink /Sim-Power System digital simulation. All of the EV-drive scheme subsystem components used in the effective Lithium-ion battery-powered PMDC motors used in the electric vehicle are sub-modelled individually using the MATLAB /Simulink /Sim-power System software environment and combined to establish the overall system model. The simulation of the proposed scheme has been carried out and the dynamic performance of the system is examined.

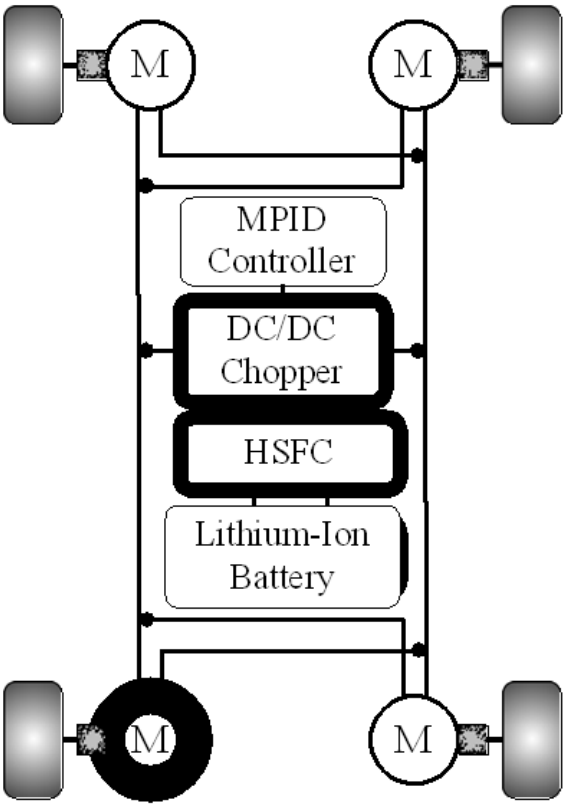

Fig.1. Schematic diagram of the proposed all-wheel PMDC drive electric vehicle.

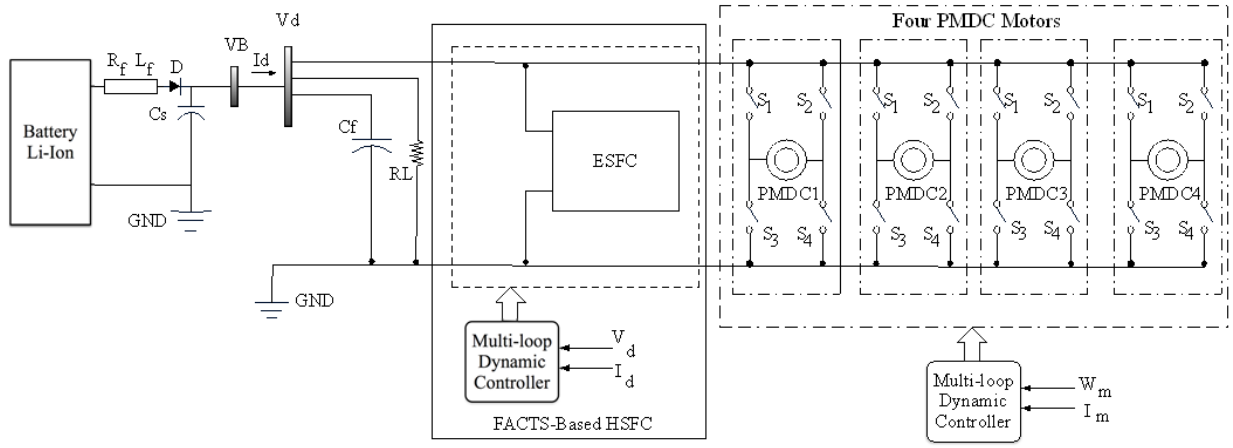

Fig.2. Schematic diagram of the all-wheel PMDC drive electric vehicle.

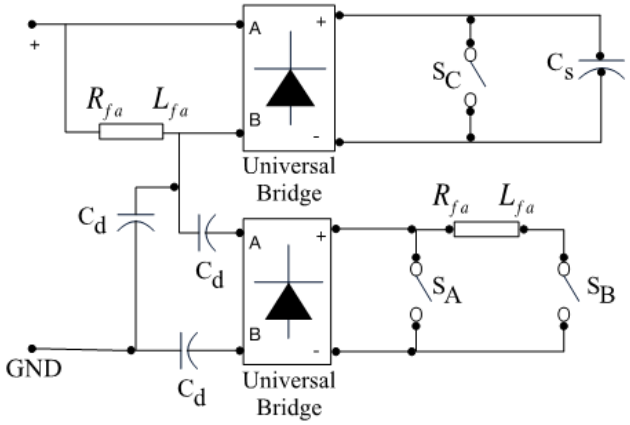

Fig.3. Efficient switched filter compensator (ESFC) for DC Bus.

IV. PMDC MOTOR

Permanent magnet DC motors are useful in a range of applications, from battery powered devices like wheelchairs and power tools, to conveyors and door openers, welding equipment, X-ray and tomographic systems, and pumping equipment, to name a few. They are frequently the best solution to motion control and power transmission applications where compact size, wide operating speed range, ability to adapt to a range of power sources or the safety considerations of low voltage are important. Their ability to produce high torque at low speed make them suitable substitutes for gear motors in many applications. Because of their linear speed-torque curve, they particularly suit adjustable speed and servo control applications where the motor will operate at less than 5000 rpm Inside these motors, permanent magnets bonded to a flux- re-turn ring replace the stator field windings found in shunt motors. A wound armature and mechanical brush commutation system complete the motor. The permanent magnets supply the surrounding field flux, eliminating the need for external field current. The block diagram of the PMDC motor is illustrated in Figure (4). The parameters and symbols, which were used in simulating the system, are given in Appendix. The armature coil of the DC motor can be represented by an inductance (L_m) in series with resistance (R_m) and with a series induced voltage (e_m), which opposes the voltage source. Using Kirchhoff's voltage law around the electrical loop can derive a differential equation for the equivalent circuit.

$$V_m(k) = R_m i_a(k) + L_m \frac{di_a}{dt} + e_m(k) \quad (1)$$

where $e_m(k) = K_E \cdot \omega_m(k)$, $i_a =$ Constant; there for $K_E = K_T$

$$T_e(k) - J\frac{d\omega_m(k)}{dt} - B\omega_m(k) - T_L(k) = 0 \quad (2)$$

The electromagnetic torque is proportional to the current though the armature winding and can be written as

$$T_e(k) = K_T i_a \quad (3)$$

The load torque is given by the nonlinear equation

$$T_L(k) = 238.73 \quad (4)$$

Where, the coefficients and are chosen as given in the Appendix. The differential equations in state space form for the armature current and angular velocity can be written as

$$\frac{d}{dx}\begin{bmatrix} i_a \\ \omega_m \end{bmatrix} = \begin{bmatrix} -\frac{R_m}{L_m} & -\frac{K_T}{L_m} \\ \frac{K_T}{J} & -\frac{B}{J} \end{bmatrix}\begin{bmatrix} i_a \\ \omega_m \end{bmatrix} + \begin{bmatrix} \frac{1}{L_m} & 0 \\ 0 & -\frac{1}{J} \end{bmatrix}\begin{bmatrix} V_m \\ T_L \end{bmatrix} \quad (5)$$

Where I_a and ω_m are motor armature current and speed. The values of the parameters used in PMDC motor modelling are given in the Appendix. Load torque is taken as generalized nonlinear torque term [19].

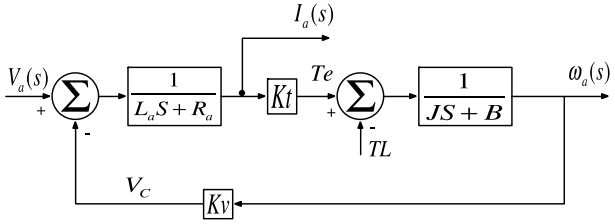

Fig.4. The block diagram of the PMDC motor

V. CONTROL STRATEGY

In this paper, a new modified tri-loop time-descaled error- driven dynamic controller scheme shown in Figure 6 is implemented for speed control of the PMDC motors. It comprises three basic loops, namely the main speed stabilization loop, the motor current dynamic error loop, and the supplementary dynamic momentum-tracking loop. The additional dynamic loops ensure energy efficient utilization and reduced current ripple content. The new modified tri-loop error-driven dynamic controller scheme shown in Figure 5 is implemented for ESFC to control and absorb ripple and reduce DC side current oscillations. The scheme comprises three basic loops, namely the main voltage stabilization loop, current dynamic error loop, and the power loop. The key parameters of the controller scheme are given in the Appendix.

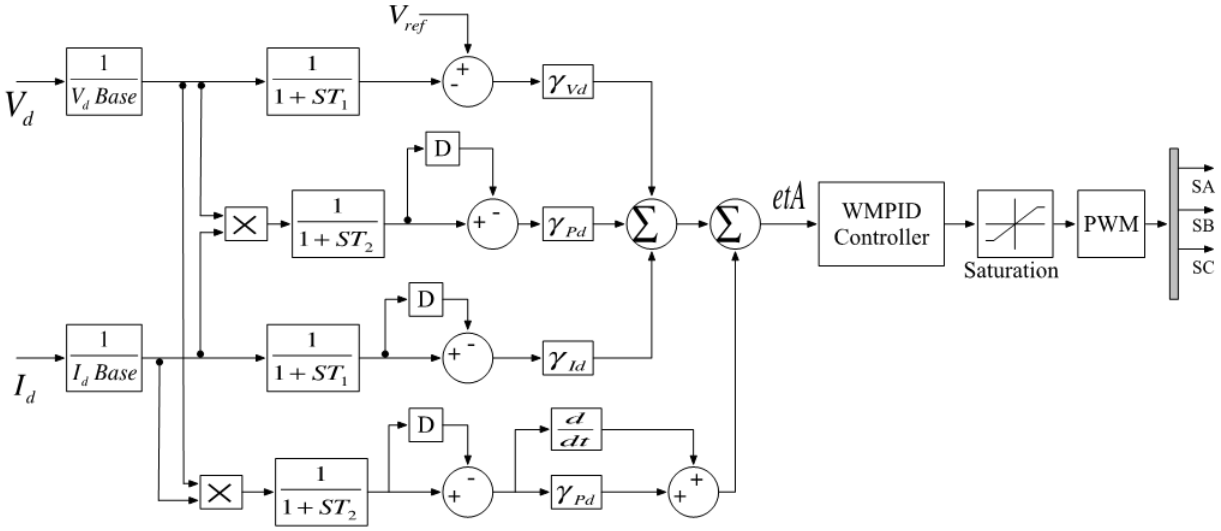

Fig.5. Tri-loop error-driven time-descaled WMPID dynamic controller for the common DC side ESFC scheme.

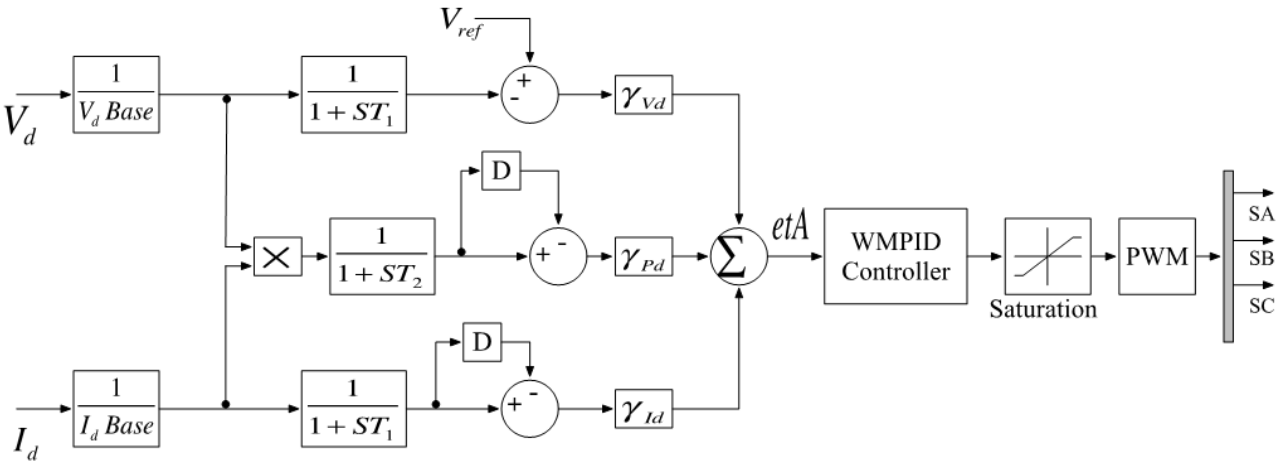

Fig.6. Tri-loop error-driven time-descaled WMPID dynamic controller for speed control reference tracking.

The total error signals (e_tA) and (e_tB) are the sum of these three basic dynamically-scaled loop errors represented by:

$$e_tA = (\gamma_{Vd} \cdot e_{Vd} + \gamma_{Pd} \cdot e_{Pd} + \gamma_{Id} \cdot e_{Id}) \quad (6)$$

$$e_tB = (\gamma_{\omega m} \cdot e_{\omega m} + \gamma_{M\omega} \cdot e_{M\omega} + \gamma_{\mathrm{Im}} \cdot e_{\mathrm{Im}}) \quad (7)$$

The system control signal has the following form in the time

$$V_c(t) = K_p \cdot e_t(t) + K_i \cdot \int_0^t e_t \cdot dt + K_d \frac{de_t(t)}{dt} + \gamma_R \cdot (e_t(t))^2 + \gamma_e \cdot (e_t(t) - e_t(t-\tau)) \quad (8)$$

The tri-loop error-driven switched filter controller compensates for any dynamic oscillations in Bus voltage and motor current on the DC Bus. The loop weighting factors are assigned to ensure loop time scaling and dominant loop control action. The total error signal to ensure maximum power utilization of the tri-loop is driven through the WMPID controller that is used to compensate the dynamic total error in order to provide the control signals, which are then used to control ESFC. The control signals are then sent to the PWM generator through saturation to adjust the sequence of the IGBT/Diode switch triggering, which is shown in Figure 7. The control

gains (Kp, Ki, Kd, γ_e and γ_R) are selected to minimize an objective function, which is used for flicker migration, voltage stabilization enhancement, efficient energy utilization, and controlling the speed of PMDC motors. The tri-loop dynamic controller is validated for voltage stabilization and dynamic reactive compensation using the MATLAB/SIMULINK/Sim-Power System toolbox software environment.

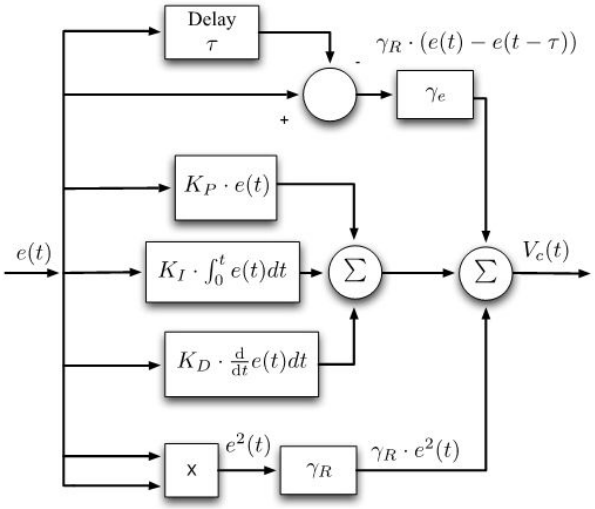

Fig.7. New WMPID dynamic controller with error-squared compensation loop.

VI. Pulse Width Modulation

Pulse width modulation (PWM) switching strategy, as it applies to motor control, is a way of delivering energy through a succession of pulses rather than a continuously varying (analog) signal. By increasing or decreasing pulse width, the controller regulates energy flow to the motor shaft. The motor's own inductance acts like a filter, storing energy during the ON cycle while releasing it at a rate corresponding to the input or reference signal. In other words, energy flows into the load not so much at the switching frequency, but at the reference frequency. PWM is somewhat like pushing a playground-style merry-go-round. The energy of each push is stored in the inertia of the heavy platform, which accelerates gradually with harder, more frequent, or longer-lasting pushes.

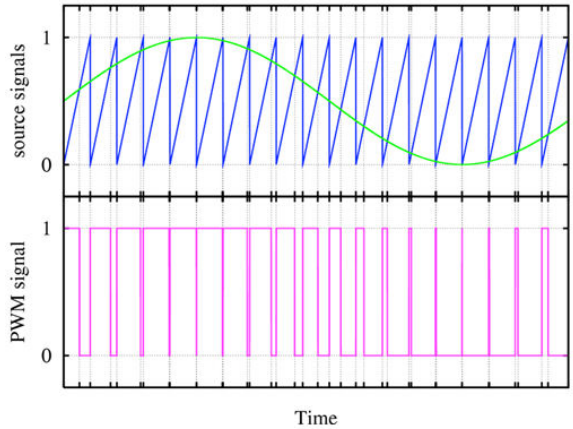

Fig.8. The pulse width modulation waveforms.

The kinetic energy is received in a very different manner than how it is applied [20], [21], [22]. The main advantage of PWM switching strategy is that power loss in the switching devices is very low. When a switch is OFF, there is practically no current, and when it is ON, there is almost no voltage drop across the switch. Power loss, being the product of voltage and current, is thus in both cases close to zero. PWM also works well with digital controls, which, because of their ON/OFF nature, can easily set the needed duty cycle. Figure 8 shows the waveforms of PWM.

VII. Digital Simulation Results

A Lithium-ion battery scheme is used to power four PMDC motors' torque disturbances. EV-PMDC motor speed response and error for the different speed tracks using WMPID controller is shown in Figures 14, 17, 20, 23. The dynamic motor torque is changed by changing the speed trajectory. Figures 15, 18, 21, 24 show the EV-PMDC motor electrical torque and current for different speed trajectories using WMPID controller. Motor speed vs. electrical torque T_e and motor speed vs. electrical torque Te vs. motor current I_a for different speed tracking are shown in Figures 16, 19, 22, 25. The Lithium-ion battery source is controlled using the tri-loop error-driven dynamic action filter using ESFC. Figures 9 - 11 show the MATLAB digital simulation results without and with the ESFC device for the voltage, current, and power at both Buses VB and VD. At the same time, Figure 12 - 13 show the MATLAB digital simulation results without and with the ESFC device for the voltage and the current total harmonic distortion (THD) % at both Buses VB and VD. Figures 26 - 27 show the simulation results with the ESFC for the voltage and current at VB and VD Buses under open circuit (OC) fault for 300 ms. The simulation results with the ESFC for the voltage and current at VB and VD Buses under short circuit (SC) fault for 100 ms are shown in Figures 28 - 29. Figures 30 - 31 show the simulation results with and without the ESFC for the voltage and current at VB and VD buses under R_L load changing. The simulation results with the ESFC for the voltage and current at VB and VD Buses under PMDC-drive torque changing are shown in Figures 32 - 33. EV-PMDC motor speed response, error, electrical torque, and current for the first speed track under T_L changing using WMPID controller are shown in Figures 34, 35. All the results indicated that the proposed modified controller is far superior compared to not using the controller in damping current and voltage excursions. The digital simulation results without and with the controlled ESFC device located at the VD Bus are used to show the voltage damping performance and Bus voltage regulation. The controller effectiveness in tracking different speed reference trajectories was tested for step reference and other trajectories.

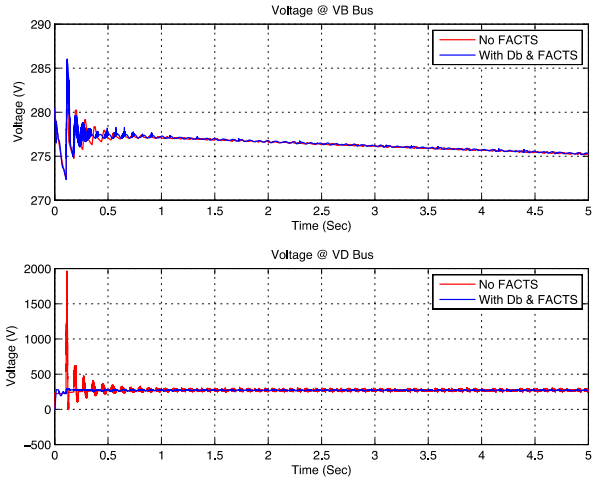

Fig.9. Digital simulation results without and with ESFC for the voltage on VB and VD Buses under normal conditions.

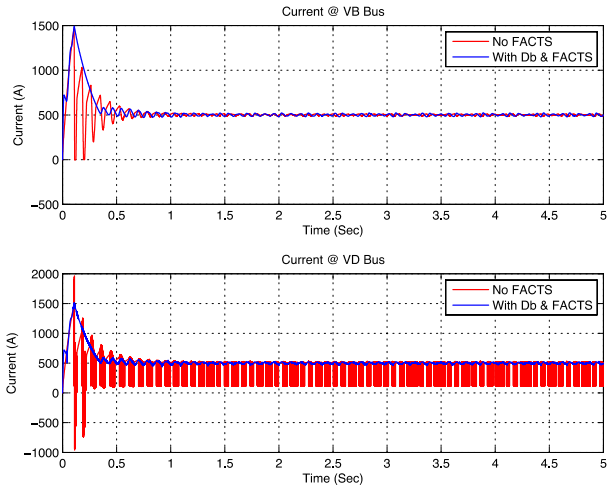

Fig.10. Digital simulation results without and with ESFC for the current on VB and VD Buses under normal conditions.

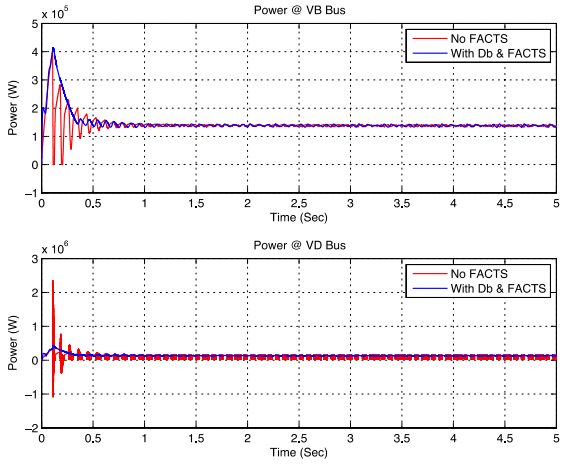

Fig.11. Digital simulation results without and with ESFC for the power on VB and VD Buses under normal conditions.

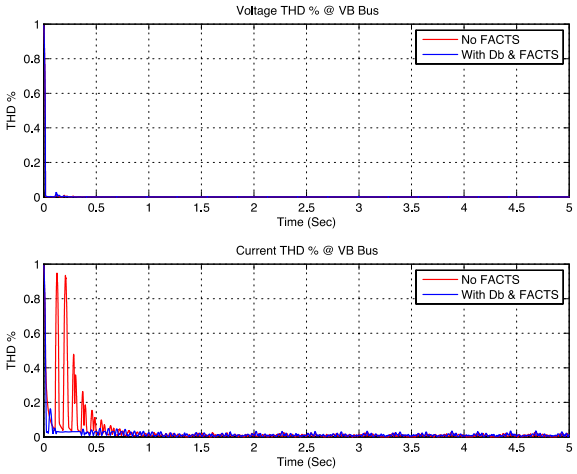

Fig.12. Digital simulation results without and with ESFC for voltage and current THD % on VB Bus under normal conditions.

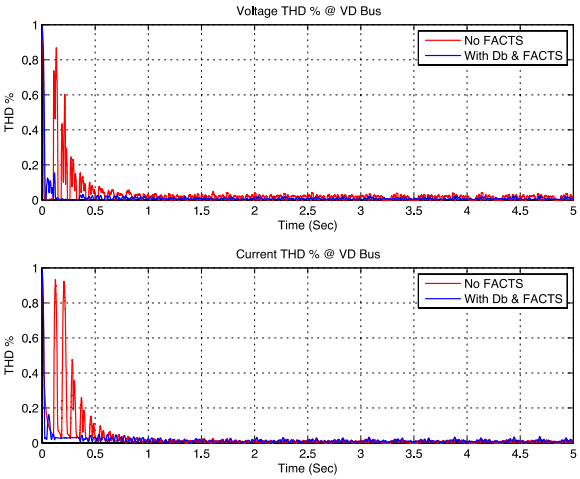

Fig.13. Digital simulation results without and with ESFC for voltage and current THD % on VD Bus under normal conditions.

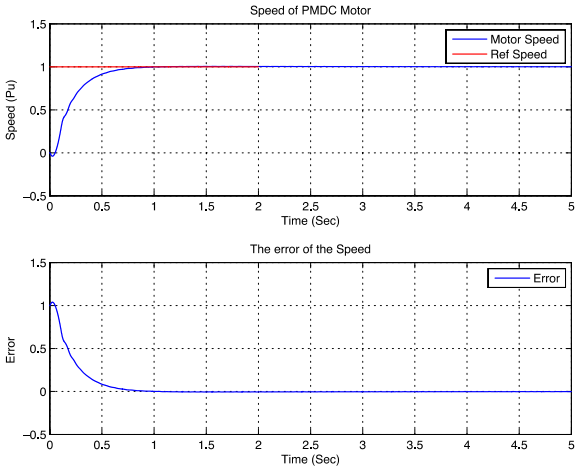

Fig. 14: Motor speed response and speed error for the first speed tracking.

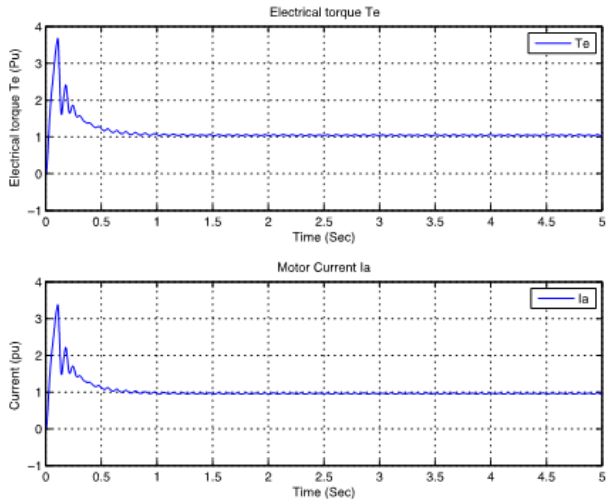

Fig.15. Motor electrical torque T_e and motor current I_a response for the first speed tracking.

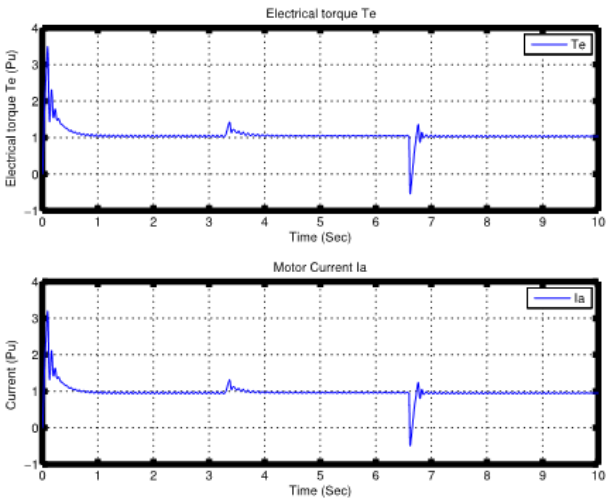

Fig.18. Motor electrical torque T_e and motor current I_a response for the second speed tracking.

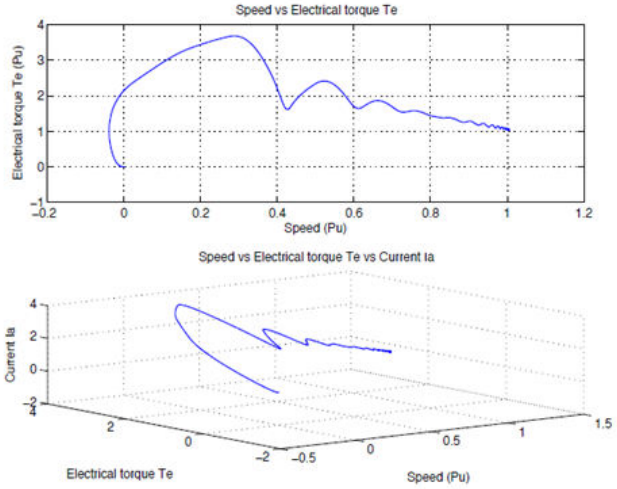

Fig.16. Motor speed vs. electrical torque T_e, and motor speed vs. electrical torque T_e vs. motor current Ia for the first speed tracking.

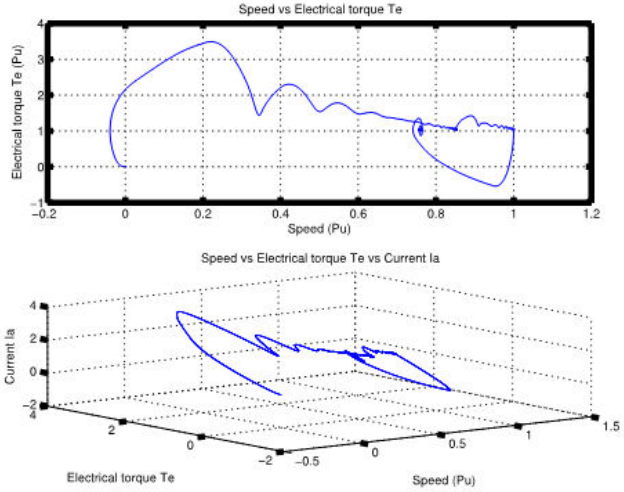

Fig.19. Motor speed vs. electrical torque T_e, and motor speed vs. electrical torque T_e vs. motor current I_a for the second speed tracking.

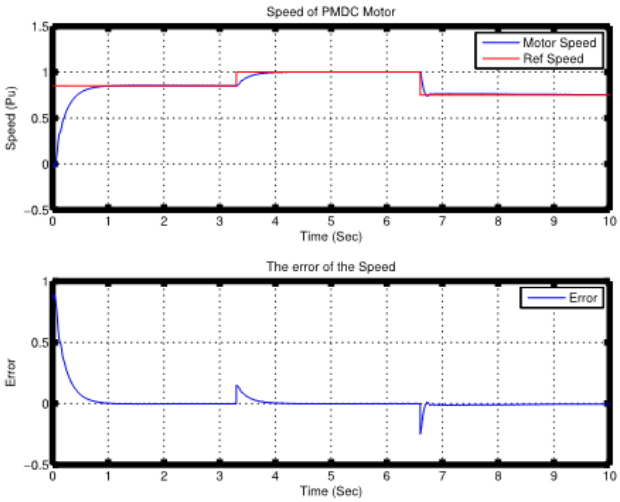

Fig.17. Motor speed response and error for the second speed tracking.

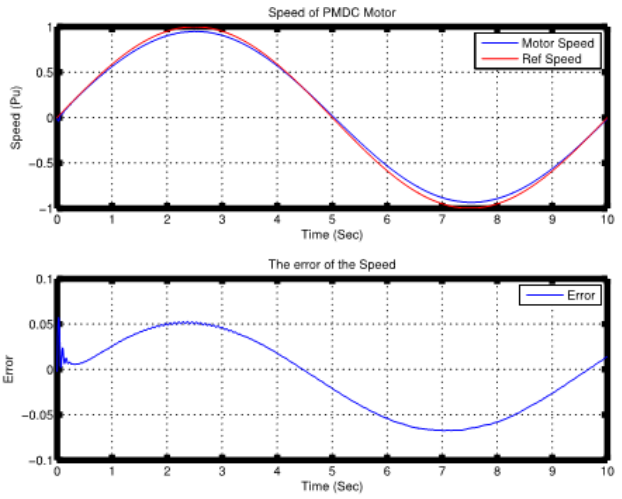

Fig.20. Motor speed response and error for the third speed tracking.

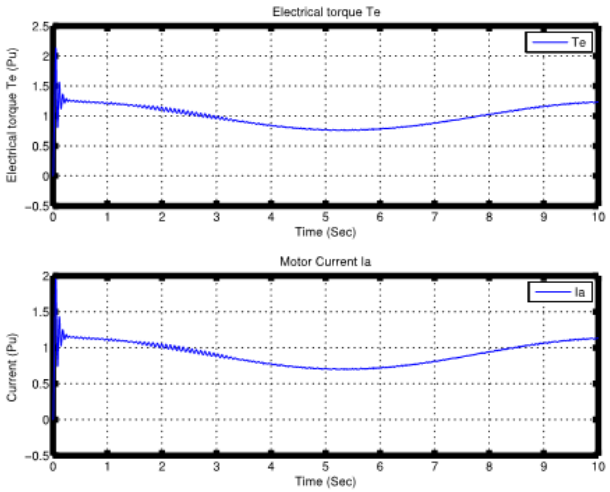

Fig. 21: Motor electrical torque T_e and motor current I_a response for the third speed tracking.

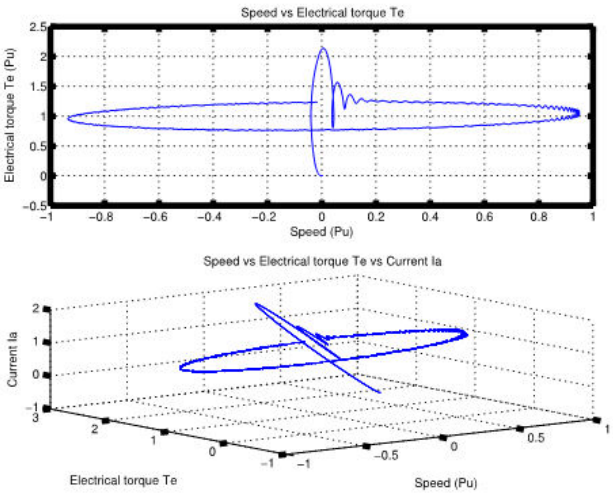

Fig.22. Motor speed vs. electrical torque T_e, and motor speed vs. electrical torque T_e vs. motor current I_a for the third speed tracking.

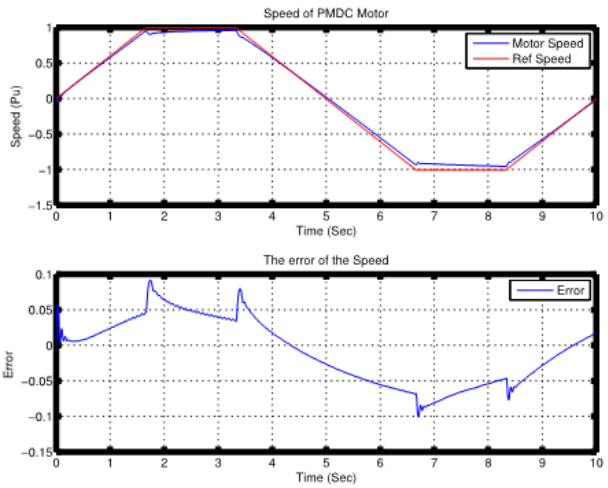

Fig.23. Motor speed response and error for the fourth speed tracking.

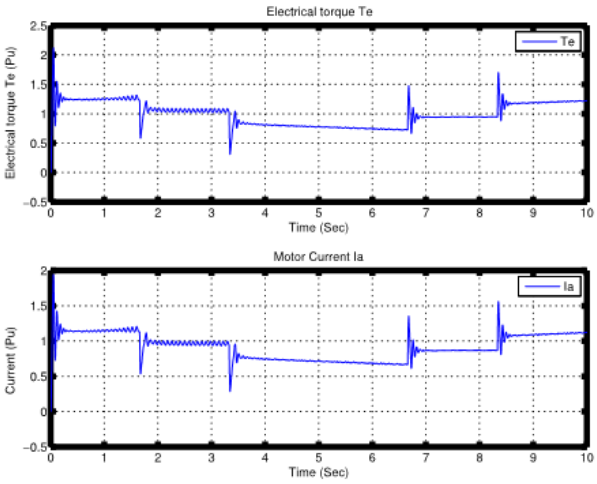

Fig.24. Motor electrical torque T_e and motor current I_a response for the fourth speed tracking.

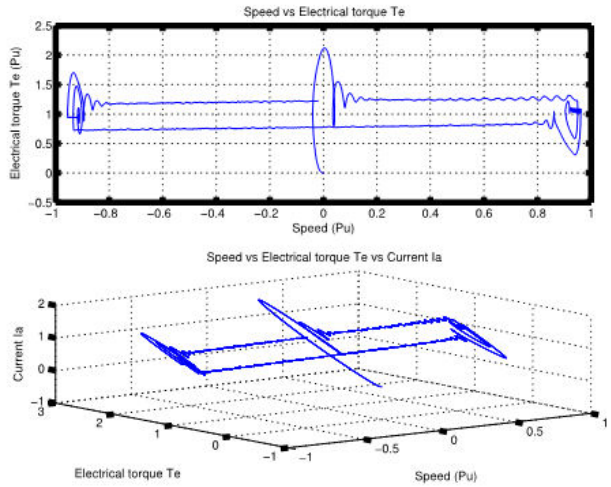

Fig.25. Motor speed vs. electrical torque T_e, and motor speed vs. electrical torque T_e vs. motor current I_a for the fourth speed tracking.

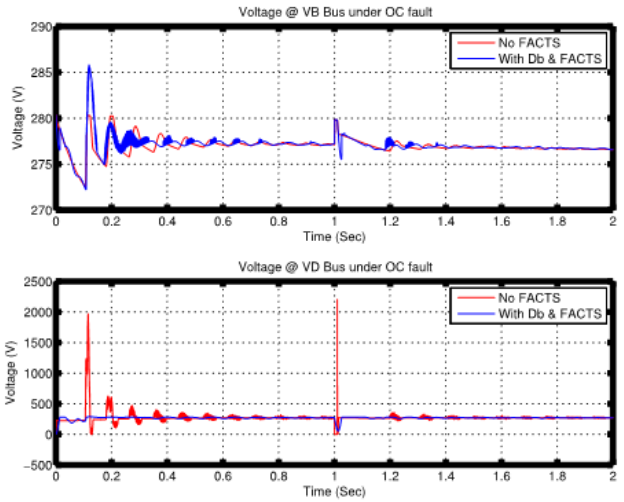

Fig.26. Digital simulation results without and with ESFC for the voltage on VB and VD Buses under OC fault condition.

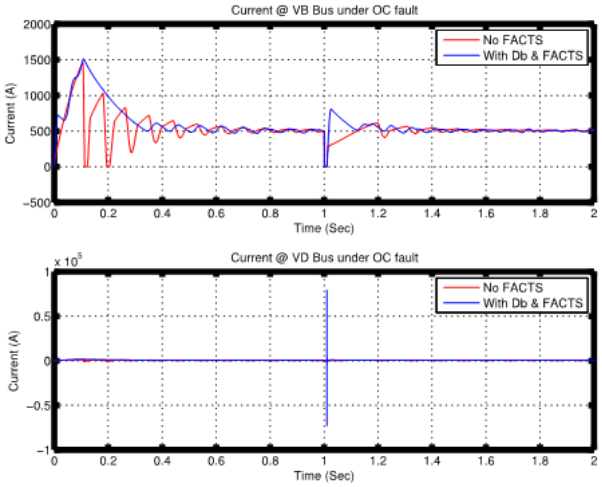

Fig.27. Digital simulation results without and with ESFC for the current on VB and VD Buses under OC fault condition.

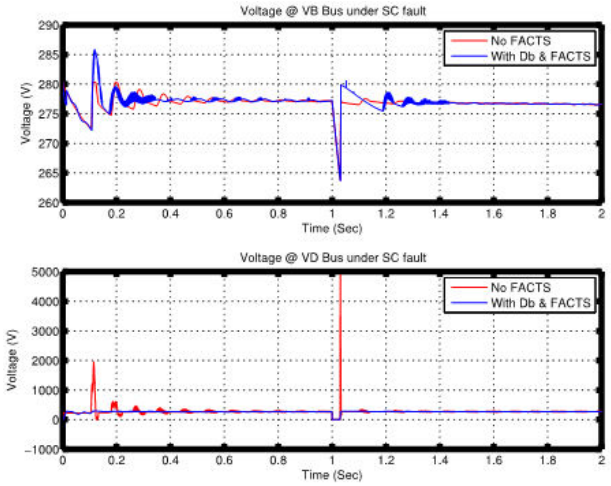

Fig.28. Digital simulation results without and with ESFC for the voltage on VB and VD Buses under SC fault condition.

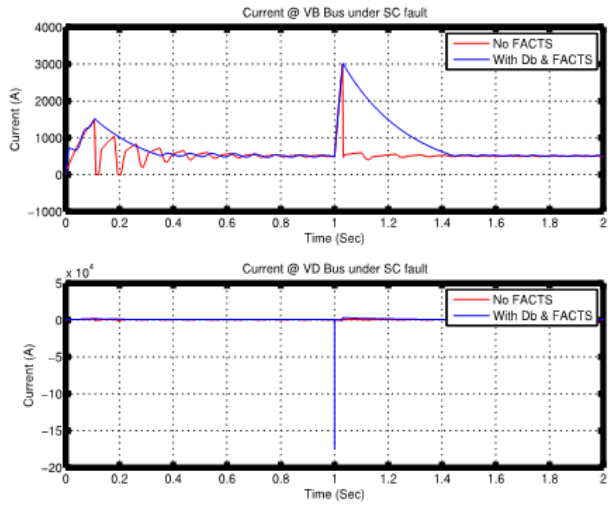

Fig.29. Digital simulation results without and with ESFC for the current on VB and VD Buses under SC fault condition.

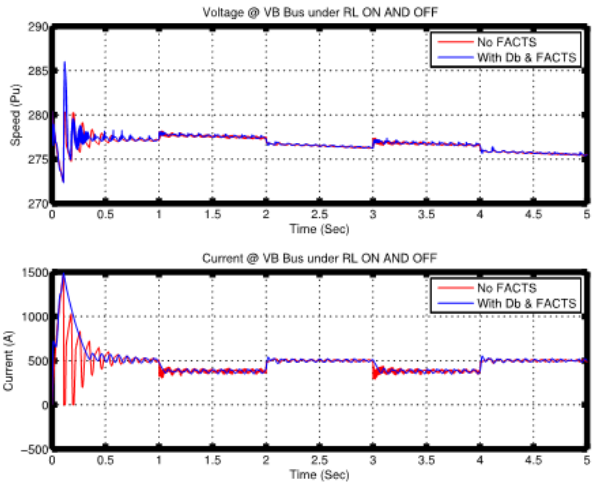

Fig.30. Digital simulation results without and with ESFC for the voltage and current on VB Bus under R_L load changing condition.

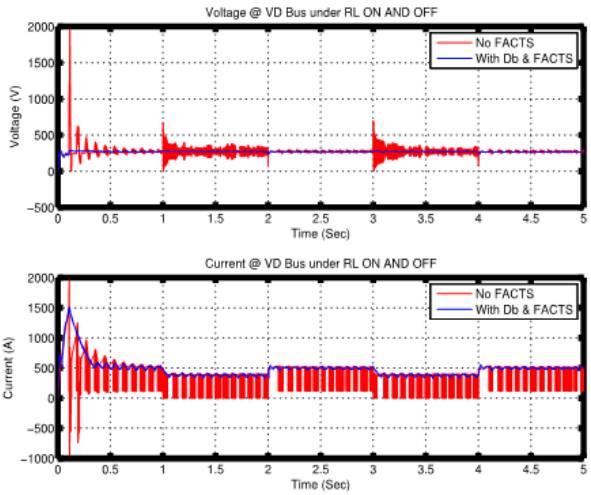

Fig.31. Digital simulation results without and with ESFC for the voltage and current on VD Bus under R_L load changing condition.

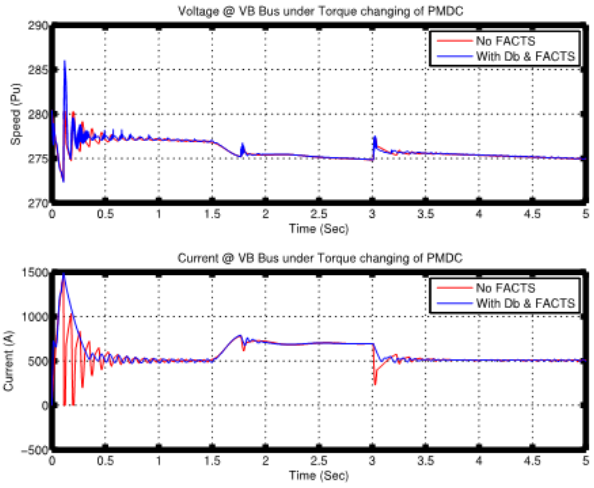

Fig.32. Digital simulation results without and with ESFC for the voltage and current on VB Bus under T_L changing condition.

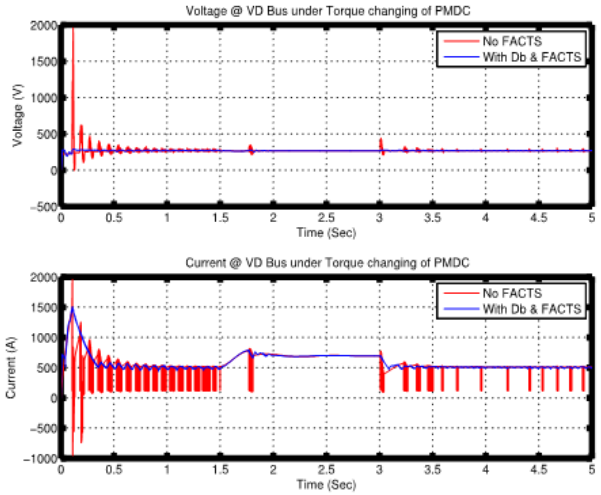

Fig.33. Digital simulation results without and with ESFC for the voltage and current on VD Bus under T_L changing condition.

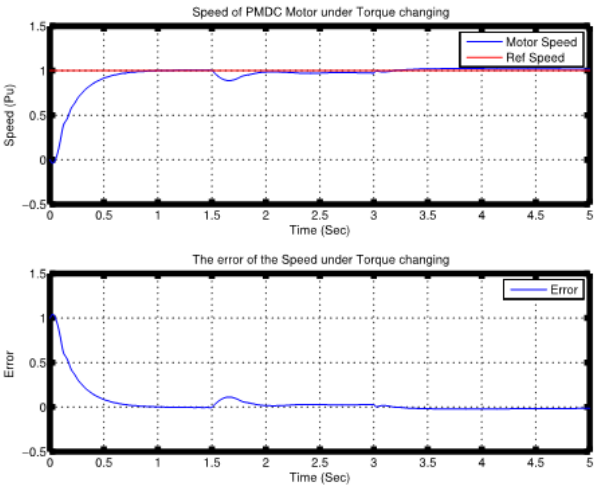

Fig. 34: Motor speed response and error for the first speed tracking under T_L changing condition.

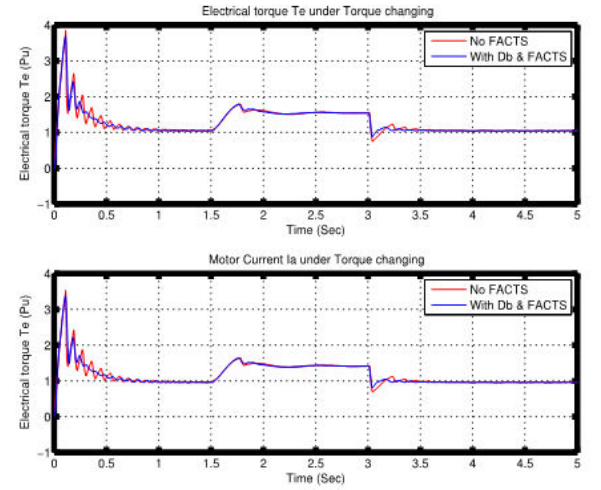

Fig.35. Motor electrical torque T_e and motor current I_a response for the first speed tracking under T_L changing condition.

VIII. CONCLUSION

A Lithium-ion battery-powered PMDC-EV drive scheme with dynamic multi-regulator control strategy is fully validated using the MATLAB/Simulink/Sim-Power System software environment. The common DC Bus scheme feeds power from a Lithium-ion battery to a four-quadratic DC/DC converter to regulate the PMDC motor all-wheel drive and the ESFC. The FACTS-based efficient switched filter compensator and control strategy ensure voltage stability with damped inrush current conditions under battery and hybrid load excursions. The Lithium-ion battery powered EV's drive excursions are fully compensated for using the ESFC and coordinated inter-coupled multi-loop error-driven dynamic controller. This ensures efficient battery source operation. The paper also presents a WMPID controller with error-squared compensation to control the four-quadrant DC/DC converter pulse width modulation as well as the ESFC using a dual regulation dynamic error-driven time-descaled WMPID multi-loop controller. The Lithium-ion battery-powered EV with all-wheel DC drive with the tri-loop dynamic error-driven speed regulator is used to track reference speed with minimal inrush currents and overloading conditions. The four-quadratic DC/DC converter is employed to match and control the power transfer from the Lithium- ion battery source to the four PMDC motors. The unified DC electric drive system is validated using the MATLAB/Simulink/Sim-Power System software environment under DC load excursion and sudden motor torque changes. The Lithium- ion battery drive system with the ESFC and multi-regulator error-driven multi-loop controller were validated for the efficient utilization of Lithium-ion battery and dynamic speed reference tracking with minimal overshoot, inrush currents, and overload current conditions.

APPENDIX

Parameter	*Value*
R_f	0.01Ω
R_s	0.15Ω
R_L Load	25Kw
L_f	3mH
L_s	3mH
C_s	200μF
C_{s1}	500μF
C_f	8500μF
C_d	8000μF
PMDC motor	*Value*
R_a	0.005Ω
L_a	0.012H
K_e	0.6366N.m/A
J	0.25Kg.m^2
B_m	0.03N.m.s
Lithium-ion Battery	*240V, 450Ah, S.O.C %100*

REFERENCES

[1] S.-i. Sakai, H. Sado, and Y. Hori, "Motion control in an electric vehicle with four independently driven in-wheel motors," *Transactions on Mechatronics (IEEE/ASME)*, vol. 4, no. 1, pp. 9–16, 1999.

[2] E. Elbakush and A. Sharaf, "A Hybrid FACTS PV-Smart Grid (V2G) Battery Charging Scheme," *International Journal of Advanced Renew- able Energy Research*, vol. 1, no. 10, pp. 560–572, 2012.

[3] R. Curtin, Y. Shrago, and J. Mikkelsen, "Plug-in hybrid electric vehi- cles," *Reuters/University of Michigan, Surveys of Consumers*, 2009.

[4] A. Emadi, Y. J. Lee, and K. Rajashekara, "Power electronics and motor drives in electric, hybrid electric, and plug-in hybrid electric vehicles," *IEEE Transactions on Industrial Electronics*, vol. 55, no. 6, pp. 2237– 2245, 2008.

[5] A. Hajimiragha, C. Caizares, M. Fowler, and A. Elkamel, "Optimal Transition to Plug-In Hybrid Electric Vehicles in Ontario, Canada, Considering the Electricity-Grid Limitations," *IEEE Transactions on Industrial Electronics*, vol. 57, no. 2, pp. 690–701, Feb. 2010.

[6] O. Tremblay and L.-A. Dessaint, "Experimental validation of a battery dynamic model for EV applications," *World Electric Vehicle Journal*, vol. 3, pp. 13–16, 2009.

[7] A. Sharaf and B. Khaki, "Novel switched capacitor-filter compensator for smart grid-electric vehicle charging scheme," in *Proceedings of the IEEE International Conference on Smart Grid Engineering (SGE'12)*, 2012, pp. 1–5.

[8] C. Mi, M. A. Masrur, and D. W. Gao, "Plug-in hybrid electric vehicles," *Hybrid Electric Vehicles: Principles and Applications with Practical Perspectives*, pp. 107–138.

[9] S. Han, S. Han, and K. Sezaki, "Development of an optimal vehicle-to- grid aggregator for frequency regulation," *IEEE Transactions on Smart Grid*, vol. 1, no. 1, pp. 65–72, 2010.

[10] K. Morrow, D. Karner, and J. Francfort, "Plug-in hybrid electric vehicle charging infrastructure review," *US Department of Energy-Vehicle Technologies Program*, 2008.

[11] J. Peas Lopes, P. R. Almeida, and F. Soares, "Using vehicle-to-grid to maximize the integration of intermittent renewable energy resources in islanded electric grids," in *International Conference on Clean Electrical Power*. IEEE, 2009, pp. 290–295.

[12] N. Parspour, "Novel drive for use in electrical vehicles," in *61st Vehicular Technology Conference (VTC 05-Spring)*, vol. 5. IEEE, 2005, pp. 2930–2933.

[13] A. Sharaf, E. Elbakush, and I. Altas, "Novel Control Strategies For Photovoltaic Powered PMDC Motor Drives," in *Canada Electrical Power Conference (EPC'07)*. IEEE, 2007, pp. 461–466.

[14] G. H. Jung and G. H. Cho, "New power active filter with simple low cost structure without tuned filters," in *29th Annual IEEE Power Electronics Specialists Conference (PESC 98 Record)*, vol. 1. IEEE, 1998, pp. 217–222.

[15] A. M. Sharaf and G. Wang, "Wind energy system voltage and energy enhancement using low cost dynamic capacitor compensation scheme," in *Proceedings of the IEEE International Conference on Electrical, Electronic and Computer Engineering*, 2004, pp. 804–807.

[16] A. Sharaf and K. Abo-Al-Ez, "A FACTS based Dynamic Capacitor Scheme for Voltage Compensation and Power Quality Enhancement," in *IEEE International Symposium on Industrial Electronics*, vol. 2. IEEE, 2006, pp. 1200–1205.

[17] A. M. Sharaf, W. Wang, and I. H. Altas, "A novel modulated power filter compensator for distribution networks with distributed wind energy," *International Journal of Emerging Electric Power Systems*, vol. 8, no. 3, 2007.

[18] A. Sharaf and R. Chhetri, "A Novel Dynamic Capacitor Compensator/Green Plug Scheme for 3Phase-4 Wire Utilization Loads," in *Canadian Conference on Electrical and Computer Engineering (CCECE'06)*. IEEE, 2006, pp. 454–459.

[19] E. Elbakush, A. Sharaf, and I. Altas, "An Efficient Tri-Loop Controller for Photovoltaic Powered Four-Wheel Electric Vehicle," in *4th International Conference on Innovations in Information Technology (IIT '07)*, 2007, pp. 421–425.

[20] H. Patangia and S. N. G. Gourisetti, "A harmonically superior switching modulator with wide baseband and real-time tunability," in *International Symposium on Electronic System Design (ISED)*. IEEE, 2011, pp. 18– 23.

[21] D. G. Holmes and T. A. Lipo, *Pulse width modulation for power converters: principles and practice*. John Wiley & Sons, 2003, vol. 18.

[22] H. Patangia and S. N. G. Gourisetti, "Real time harmonic elimination using a modified carrier," in *22nd International Conference on Electrical Communications and Computers (CONIELECOMP)*. IEEE, 2012, pp. 273–277.

AUTHOR'S PROFILE

E. Elbakush

obtained his B.Sc. degree in Electrical Engineering from Bright Star University of Technology, Mersa El-Brega, Libya in 1990. He completed his M.Sc. degree in Electrical Engineering in 2000 from Budapest University of Technology and Economics, H- 1521 Budapest, Hungary. He is currently seeking his PhD degree in Electrical engineering at the University of New Brunswick, Fredericton, and NB, CANADA. He worked as Instructor with University of Seventh April, Libya for 3 years. His research areas are V2G and V2H smart grid application, and FACTS technology application in renewable energy interfacing.

A. M. Sharaf

obtained his B.Sc. degree in Electrical Engineering from Cairo University in 1971. He completed an M.Sc. degree in Electrical engineering in 1976 and PhD degree in 1979 from the University of Manitoba, Canada and was employed by Manitoba Hydro as Special Studies Engineer, responsible for engineering and economic feasibility studies in Electrical Distribution System Planning and Expansion. Dr. Sharaf was selected as NSERC- Canada Research-Assistant Professor in 1980 at University of Manitoba. He joined the University of New Brunswick in 1981 to start a tenure-track academic career as an Assistant professor and he was promoted to Associate Professor in 1983, awarded tenure in 1986, and the full professorship in 1987. Dr. Sharaf has extensive industrial and consulting experience with Electric Utilities in Canada and Abroad. He authored and co-authored over 695 scholarly Technical Journal, Referred Conference Papers, and Engineering Reports. Dr. Sharaf holds a number of US and International Patents (Pending) in electric energy, electro- technology and environmental devices He supervised over (52) Graduate Student (37-M.Sc & 13-Ph.D.) since joining Academia in July-1981.